Article

# Liquid Hydrogen in Protonic Chabazite

Adriano Zecchina, Silvia Bordiga, Jenny G. Vitillo, Gabriele Ricchiardi, Carlo Lamberti, Giuseppe Spoto, Morten Bjrgen, and Karl Petter Lillerud

*J. Am. Chem. Soc.*, **2005**, 127 (17), 6361-6366• DOI: 10.1021/ja050276c • Publication Date (Web): 12 April 2005



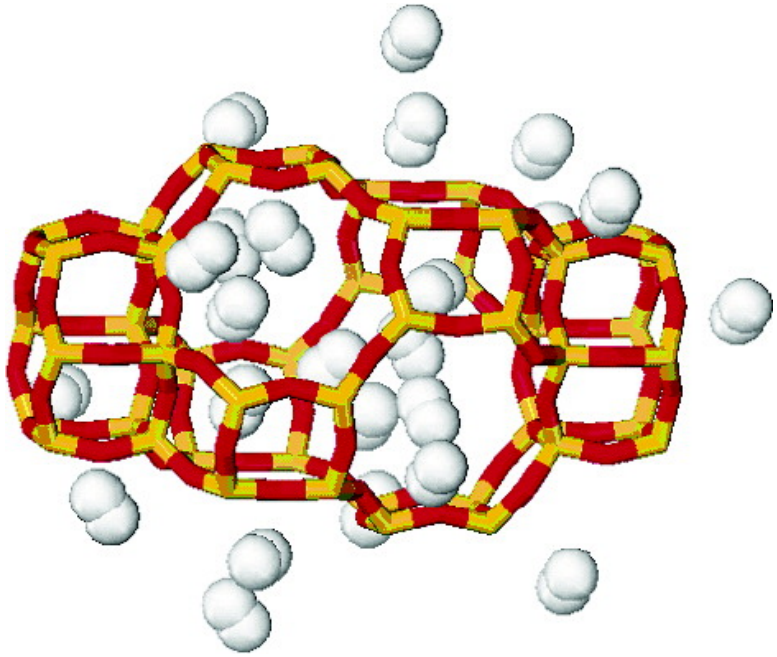

J|A|C|S
ARTICLES
Published on Web 04/12/2005

# Liquid Hydrogen in Protonic Chabazite

Adriano Zecchina,[†] Silvia Bordiga,*[,†] Jenny G. Vitillo,[†] Gabriele Ricchiardi,[†] Carlo Lamberti,[†] Giuseppe Spoto,[†] Morten Bjørgen,[‡] and Karl Petter Lillerud[‡]

*Contribution from the Dipartimento di Chimica IFM and NIS Centre of Excellence, Via P. Giuria 7, I-10125 Torino, Italy, and Department of Chemistry, University of Oslo, P.O. Box 1033, N-0315 Oslo, Norway*

Received January 15, 2005; E-mail: silvia.bordiga@unito.it

***Abstract:*** Due to its fully reversible nature, $H_2$ storage by molecular adsorption could represent an advantage with respect to dissociative processes, where kinetic effects during the charging and discharging processes are present. A drawback of this strategy is represented by the extremely weak interactions that require low temperature and high pressure. High surface area materials hosting polarizing sites can represent a viable way toward more favorable working conditions. Of these, in this contribution, we have studied hydrogen adsorption in a series of zeolites using volumetric techniques and infrared spectroscopy at 15 K. We have found that in H-SSZ-13 zeolite the cooperative role played by high surface area, internal wall topology, and presence of high binding energy sites (protons) allows hydrogen to densify inside the nanopores at favorable temperature and pressure conditions.

## 1. Introduction

The worldwide approach to hydrogen as a sustainable energy carrier challenges a diversity of scientific communities to address the problems of hydrogen production, transport, storage, and fuel cell technology.[1−3] Devoted basic research and new breakthroughs are indeed required before hydrogen-based energy systems can be envisaged.[4]

At room temperature and atmospheric pressure, hydrogen occupies about 3000 times the volume of gasoline providing the same amount of energy. Thus, for any practical purpose, hydrogen has to be mechanically compressed, liquefied, or subjected to some other more sophisticated storage method.[1,5,6] Today, the prototype hydrogen vehicles use space-demanding tanks with compressed gas. Energy density considerations certainly make hydrogen liquefaction attractive, but it requires cryogenic temperature, whose achievement consumes about 30% of the energy carried by hydrogen. An additional complication will be the weight of the extensively insulated tanks and the continuous loss of hydrogen at RT.

Materials interesting as hydrogen reservoirs should provide a secure, light, and cheap storage. They should furthermore possess a high sorption capacity and the fastest possible recharging kinetics.[6] Many storage strategies have been followed in recent years, aiming at fulfilling these requirements. The most important ones are: (1) storage in metals and alloys; (2) storage in complex hydrides (alanates, borides); (3) storage by trapping (e.g., in clathrates); and (4) storage in microporous materials (carbons, metal−organic frameworks, polymers, zeolitic materials).

Storage in metals, alloys, and in complex hydrides involves chemical forces.[7] They can be considered promising only when the involved enthalpies are sufficiently low to allow charging and discharging at temperatures close to ambient and pressures not higher than those reached by compressors. Kinetics problems are also of paramount importance for these systems because charging and discharging involve the surface dissociation of hydrogen molecules or surface recombination of hydrogen atoms that are both activated processes.

Clathrates,[8] some small pore zeolites,[9] and new metal−organic frameworks (MOFs)[10] can trap and release molecular hydrogen by changing the pressure and temperature conditions. High pressure is used to force hydrogen inside the cavities, then, by decreasing the temperature, the frameworks form a barrier able to keep $H_2$ entrapped. A temperature increase allows $H_2$ release.

Storage in microporous materials involves the interaction of molecular hydrogen with the internal surfaces of micropores, governing the stability of the molecular adducts and the optimal temperature of storage. The forces involved in this process are essentially physical (dispersive), and the involved enthalpies are low (e.g., 4 kJ mol$^{-1}$ for $H_2$ on graphite[7]). In this area, carbon-based materials have been widely investigated. Of these, the most promising candidates were nanostructured graphite[11] and carbon nanotubes.[1,12−14] In nanoporous solids, the dimension

[†] Dipartimento di Chimica IFM and NIS Centre of Excellence.
[‡] University of Oslo.

(1) Schlapbach, L.; Züttel, A. *Nature* **2001**, *414*, 353−358.
(2) Winter, C. J.; Nitsch, J. *Hydrogen as an Energy Carrier: Technologies, Systems, Economy*; Springer-Verlag: Berlin 1988.
(3) Steele, B. C. H.; Heinzel, A. *Nature* **2001**, *414*, 345−352.
(4) Service, R. F. *Science* **2004**, *305*, 958−961.
(5) Züttel, A. *Naturwissenschaften* **2004**, *91*, 157−172.
(6) Berry, G. D.; Aceves, S. M. *Energy Fuels* **1998**, *12*, 49−55.
(7) Seayad, A. M.; Antonelli, D. M. *Adv. Mater.* **2004**, *16*, 765−777.
(8) Florusse, L. J.; Peters, C. J.; Schoonman, J.; Hester, K. C.; Koh, C. A.; Dec, S. F.; Marsh, K. N.; Sloan, E. D. *Science* **2004**, *306*, 469−471.
(9) Weitkamp, J.; Fritz, M.; Ernst, S. *Int. J. Hydrogen Energy* **1995**, *20*, 967−970.
(10) Zhao, X. B.; Xiao B.; Fletcher, A. J.; Thomas, K. M.; Bradshaw, D.; Rosseinsky, M. J. *Science* **2004**, *306*, 1012−1015.

and the shape of the pores play a critical role in hydrogen adsorption performance.[15] Indeed, in pores having diameters not exceeding a few $H_2$ molecular radii (dynamic diameter = 4.1 Å), the potential fields from surrounding walls overlap so that the attractive force acting on hydrogen molecules will exceed that exerted by open flat surfaces. This explains the $H_2$ adsorption performance of the already mentioned carbon nanotubes[1,14] and can explain the results obtained on MOFs.[16,17] For this class of materials, only an increase in surface area can improve the $H_2$ adsorption properties because of the lack of specific interacting sites.[1] In this respect, fundamental studies on $H_2$ interactions with ions in the gas phase report high interaction energies.[18] Unfortunately, in condensed matter, cations need counterions to be stabilized and when counterions are considered, the interaction energy decreases substantially. The most prominent class of microporous materials, which contains isolated and exposed cations, are zeolites and zeotypes, already widely employed in catalysis and gas separation.[19] However, these materials are not sufficiently light to represent the final solution to $H_2$ storage. However, they can be ideal systems to investigate the interaction of $H_2$ with both dispersive and electrostatic forces. Furthermore, the availability of a large variety of frameworks and chemical compositions combined with low cost and superior mechanical and thermal stabilities increased the interest in these materials. Moreover, the possibility to perform reproducible, systematic fundamental studies gives relevance to the results obtained on this class of materials which, until now, have shown adsorptive properties inferior to those of the other microporous matrixes.[15,20−29] The study presented here is part of this research area and combines volumetric measurements (performed at 77 K in the $1 \times 10^{-7}$ to 0.92 bar range) and infrared (IR) spectroscopy (in the 15−60 K and $1 \times 10^{-7}$ to 0.013 bar ranges) on a large variety of zeolites. By combining volumetric measurements, providing quantitative data, and IR spectroscopy of adsorbed $H_2$, which is able to evaluate the number, distribution, and strength of specific interaction sites, we can make an assessment of the main aspects playing an important role in molecular $H_2$ storage. Among all of the investigated materials, those with CHA topology (namely, H-SSZ-13,[30] H-SAPO-34, and H-chabazite) have shown very good performance, and in particular, the H-SSZ-13 zeolite has shown a capacity comparable to that observed for MOFs.[16] In this work, we present in detail the data obtained on this compound, characterized by (i) high surface area, (ii) high accessible volume, divided in small and regular cavities, and (iii) presence of polarizing centers able to give specific interaction with hydrogen. The synergic role played by these three points results in the liquefaction of hydrogen inside the nanopores at favorable temperature and pressure conditions.

## 2. Materials and Experimental Section

The chabazite topology can be described as layers of double 6-rings that are interconnected by 4-rings. The double 6-ring layers stack in an ABC sequence. This leads to a framework with a regular array of barrel-shaped cages interconnected by 8-ring windows.[30] Zeolite SSZ-13 was obtained by a hydrothermal procedure described elsewhere,[31] while the topologically analogous H-SAPO-34 sample was synthesized in accordance with standard procedures[32] and calcined at 873 K in air for 4 h. The elemental composition was Si:Al:P = 1:6:5. The acidic form of SSZ-13 was obtained by a controlled calcination procedure, aiming at preserving the crystallinity of the material. The template removal was carried out in a pure oxygen flow (20 mL/min) in a fixed bed tubular quartz reactor according to the following procedure. The as-synthesized sample was initially heated to 573 K and left at this temperature for 12 h. The temperature was slowly increased to 773 K and kept isothermal for another 12 h. Powder XRD (measured on a Siemens D5000 diffractometer using Cu $K_{\alpha 1}$ radiation) confirmed a pure SSZ-13 phase. Qualitative elemental analysis and sample morphology were examined using a Philips XL 30 Scanning Electron Microscope. The Si:Al ratio was 11.6, and average particle size was in the range of 5−10 $\mu$m. Thermogravimetric analysis (TGA-DTC) of the as-synthesized sample was performed with a Rheometric Scientific STA 1500 instrument at a heating rate of 10 K/min in a pure oxygen flow.

Adsorption measurements were performed with a commercial Micromeritics ASAP 2010 sorption analyzer. Surface area has been obtained by $N_2$ adsorption at 77 K; accessible microporous volume has been estimated by the t-plot (Harkins and Jura thickness equation) of the $N_2$ adsorption data.

The infrared spectroscopic measurements were performed using a properly designed cryogenic cell allowing (i) the in situ high-temperature activation of the sample under high vacuum condition or in desired atmosphere (an activation in vacuum at 773 K has been adopted in these experiments); (ii) the performance of FTIR adsorption experiments at fixed temperature, as low as ca. 15 K (estimated at the sample level) and variable $H_2$ pressure; (iii) recording of the IR spectra of the species adsorbed in the whole from 300 to 15 K temperature interval while simultaneously measuring the gas-phase equilibrium pressure, a procedure which allows us to obtain the site-specific adsorption enthalpy. A detailed description of the cryogenic cell (consisting of a properly modified closed circuit liquid helium Oxford CCC 1204 cryostat) is given elsewhere.[33] The spectra were acquired

(11) Orimo, S.; Majer, G.; Fukunaga, T.; Zuttel, A.; Schlapbach, L.; Fujii, H. *Appl. Phys. Lett.* **1999**, *75*, 3093−3095.
(12) Dillon, A. C.; Jones, K. M.; Bekkedahl, T. A.; Kiang, C. H.; Bethune, D. S.; Heben, M. J. *Nature* **1997**, *386*, 377−379.
(13) Chen, P.; Wu, X.; Lin, J.; Tan, K. L. *Science* **1999**, *285*, 91−93.
(14) Züttel, A.; Nutzenadel, C.; Sudan, P.; Mauron, P.; Emmenegger, C.; Rentsch, S.; Schlapbach, L.; Weidenkaff, A.; Kiyobayashi, T. *J. Alloys Compd.* **2002**, *330−332*, 676−682.
(15) Nijkamp, M. G.; Raaymakers, J. E. M. J.; van Dillen, A. J.; de Jong, K. P. *Appl. Phys. A* **2001**, *72*, 619−623.
(16) Sagara, T.; Klassen, J.; Ganz, E. *J. Chem. Phys*. **2004**, *121*, 12543−12547.
(17) Rowsell, J. L. C.; Millward, A. R.; Park, K. S.; Yaghi, O. M. *J. Am. Chem. Soc.* **2004**, *126*, 5666−5667.
(18) Wu, C. H. *J. Chem. Phys.* **1979**, *71*, 783−787.
(19) Grayson, M.; Eckroth, D. *Kirk-Othmer Encyclopedia of Chemical Technology*, 3rd ed.; John Wiley & Sons: New York, 1981; Vol. 15, pp 638−669.
(20) Langmi, H. W.; Walton, A.; Al-Mamouri, M. M.; Johnson, S. R.; Book, D.; Speight, J. D.; Edwards, P. P.; Gameson, I.; Anderson, P. A.; Harris, I. R. *J. Alloys Compd.* **2003**, *356*, 710−715.
(21) Forster, P. M.; Eckert, J.; Chang, J. S.; Park, S. E.; Ferey, G.; Cheetham, A. K. *J. Am. Chem. Soc.* **2003**, *125*, 1309−1312.
(22) Guillou, N.; Gao, Q.; Forster, P. M.; Chang, J. S.; Nogues, M.; Park, S. E.; Ferey, G.; Cheetham, A. K. *Angew. Chem., Int. Ed.* **2001**, *40*, 2831−2834.
(23) Stéphanie-Victoire, F.; Goulay, A. M.; Cohen de Lara, E. *Langmuir* **1998**, *14*, 7255−7259.
(24) Kazansky, V. B.; Borovkov, V. Y.; Serich, A.; Karge, H. G. *Microporous Mater*. **1998**, *22*, 251−259.
(25) Bordiga, S.; Garrone, E.; Lamberti, C.; Zecchina, A.; Otero Areán, C.; Kazansky, V. B.; Kustov, L. M. *J. Chem. Soc., Faraday Trans.* **1994**, *90*, 3367−3372.
(26) Makarova, M. A.; Zholobenko, V. L.; Alghefaili, K. M.; Thompson, N. E.; Dewing, J.; Dwyer, J. *J. Chem. Soc., Faraday Trans.* **1994**, *90*, 1047−1054.
(27) Garrone, E.; Kazansky, V. B.; Kustov, L. M.; Sauer, J.; Senchenya, I. N.; Ugliengo, P. *J. Phys. Chem.* **1992**, *96*, 1040−1045.
(28) Otero Areán, C. Manoilova, O. V.; Bonelli, B.; Delgado, M. R.; Turnes Palomino, G.; Garrone, E. *Chem. Phys. Lett.* **2003**, *370*, 631−635.
(29) Spoto, G.; Gribov, E.; Bordiga, S.; Lamberti, C.; Ricchiardi, G.; Scarano, D. Zecchina, A. *Chem. Commun.* **2004**, 2768−2769.
(30) Smith, L. J.; Davidson, A.; Cheetham, A. K. *Catal. Lett.* **1997**, *49*, 143−146.
(31) Zones, S. I. US Patent 4 544 538, 1985, and private communication Zones, S. I.
(32) Lok, M. B.; Messina, C. A.; Patton, R. L.; Gajek, R. T.; Cannan, T. R.; Flanigen, E. M. US Patent 4 440 871, example 35 and 36, 1984.

***Table 1.*** Volumetric Measurement Values Obtained at 77 K on Zeolites and Zeotypes

| materials | framework type (IZA code) | pressure (bar) | $H_2$ uptake (mass%) | BET area ($m^2/g$) | ref |
|---|---|---|---|---|---|
| VSB-1 | | 0.79 | 0.11 | 183 | 21,22 |
| aerogel[a] | | 0.92 | 0.32 | 533 | unpublished results |
| NaY (Si/Al = 2.4) | FAU | 0.57 | 0.37 | | 24 |
| zeolite L | LTL | 1.00 | 0.53 | 344 | 15 |
| H−Y (Si/Al = 2.7) | FAU | 0.95 | 0.56 | | 26 |
| VSB-5 | | 0.79 | 0.57 | 500 | 21,22 |
| MCM-41[a] | | 1.00 | 0.58 | 1017 | 15 |
| ferrierite | FER | 1.00 | 0.58 | 344 | 15 |
| H-MOR (Si/Al = 7.0) | MOR | 0.66 | 0.60 | | 26 |
| (Mg,Na,K)-ETS-10 | | 0.92 | 0.67 | 324 | unpublished results |
| H-ZSM-5 (Si/Al = 40) | MFI | 0.92 | 0.71 | 418 | this work |
| H-ZSM5 (Si/Al = 16) | MFI | 0.66 | 0.72 | | 26 |
| silicalite | MFI | 0.92 | 0.73 | 474 | unpublished results |
| NaX (Si/Al = 1.4) | FAU | 0.55 | 0.79 | | 24 |
| (Na,K)-ETS-10 | | 0.92 | 0.80 | 337 | unpublished results |
| H-SAPO-34 | CHA | 0.92 | 1.09 | 547 | this work |
| H-chabazite (Si/Al = 2.125) | CHA | 0.92 | 1.10 | 490 | unpublished results |
| NaX (Si/Al = 1.05) | FAU | 0.61 | 1.22 | | 24 |
| NaA | LTA | 1.05 | 1.24 | | 23 |
| H-SSZ-13 | CHA | 0.92 | 1.28 | 638 | this work |

[a] Values for aerogel and MCM-41 are reported for comparison.

at a resolution of 1 $cm^{-1}$ by averaging 128 interferograms on a Bruker Equinox-55 FTIR spectrometer whose sample compartment was modified ad hoc to accommodate the cryogenic IR cell.

All volumetric and spectroscopic measurements have been preceded by activation in high vacuo at 773 K in order to remove physisorbed water and impurities. In the $H_2$ adsorption−desorption experiments, a complete reversibility of the phenomenon was observed for all samples in the whole range of pressures.

## 3. Results and Discussion

**3.1. $H_2$ Adsorption in H-SSZ-13: Volumetric Aspects.** Table 1 collects textural and adsorptive properties of selected relevant materials at 77 K and atmospheric pressure. These measurements have been performed on a large number of matrixes, mainly containing $Na^+$ ions or protons as charge balancing species. First of all, we want to underline the good reproducibility of the results, a feature that has been too often lacking in studies on carbon-based materials due to the poor structural definition of the samples. In fact, most zeolitic materials are highly crystalline, and their bulk composition can be accurately controlled. A second general observation is that within a homogeneous class of materials (zeolites and zeotypes) a large dispersion of values is observed; from the less efficient material (VSB-1) to the most active (H-SSZ-13), there is a difference of more than 1 order of magnitude (see Table 1).

The characteristics which seem to play an important role for $H_2$ uptake include the following. (i) High surface area (i.e., surface accessible to probe molecules such as $N_2$).[15,20] (ii) Role of framework topology. The presence of small nanocavities, which maximize the extension of the $H_2$ framework contact surface, seems to guarantee higher $H_2$ uptakes. Note the low $H_2$ uptake of aerogels and MCM-41 characterized by mesoporosity.[15] (iii) Presence of highly dispersed exposed polarizing species. Cations seem to be the most favorable polarizing centers able to generate a specific interaction with hydrogen via polarization and quadrupolar interactions.

Figure 1 reports $H_2$ uptake volumetric measurements, performed at 77 K in the 0−0.9 bar range for H-SSZ-13, for its aluminophosphate homologue H-SAPO-34, and for H-ZSM-5 (for comparison). The general behavior of H-SSZ-13 (full squares) and H-SAPO-34 (open squares) is very similar, but the uptake measured for H-SSZ-13 is higher than that found for H-SAPO-34 at all pressures. $H_2$ uptake of H-ZSM-5 is much lower. Another important characteristic of adsorption curves obtained for H-SSZ-13 and H-SAPO-34 is that at 0.92 bar (last point of the isotherm), they have a larger slope than that of H-ZSM-5; this suggests the possibility of substantial additional increase of $H_2$ storage with a moderate increase of the working pressure. Note that a pressure increase of 1 or 2 orders of magnitude could represent practical operating conditions in applications.

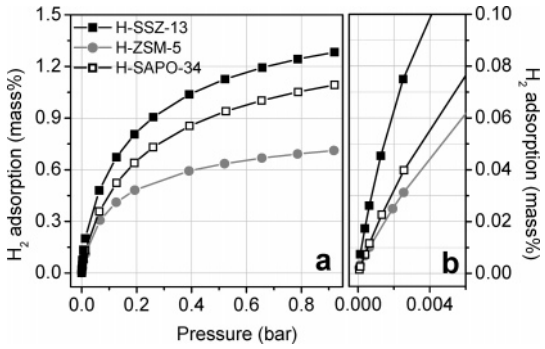


***Figure 1.*** Hydrogen gas sorption isotherms on H-ZSM-5, H-SAPO-34, and H-SSZ-13 at 77 K. (a) $1 \times 10^{-7}$ to 0.92 bar range. (b) Enlargement of the low-pressure region (in the $1 \times 10^{-7}$ to 0.006 bar range).

By looking in more detail at the isotherm behavior at low pressure (see Figure 1b where the region of 0−0.006 bar is reported), we note that H-SSZ-13 shows a steeper $H_2$ uptake. This characteristic indicates a strong affinity of the adsorbing matrix toward hydrogen.

**3.2. $H_2$ Adsorption in H-SSZ-13: Characterization of Specific Interaction Sites.** To single out the role of specific sorption sites, the isotherm obtained on H-SSZ-13 has been analyzed following the Langmuir and Dubinin models.[34] It has been evidenced that the isotherm is well described if we consider

(33) Spoto, G.; Gribov, E. N.; Ricchiardi, G.; Damin, A.; Scarano, D.; Bordiga, S.; Lamberti, C.; Zecchina, A. *Prog. Surf. Sci.* **2004**, *76*, 71−146.

(34) Dubinin, M. M.; Astakhov, V. A. *Adv. Chem. Ser.* **1971**, *102*, 69−85.

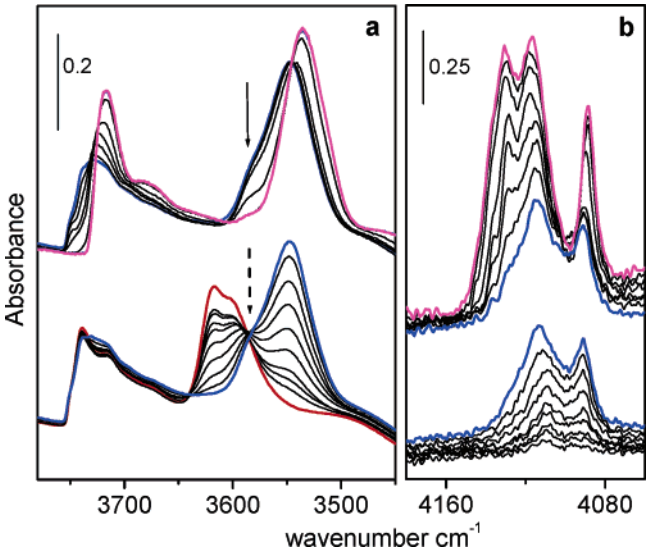


***Figure 2.*** IR spectra of $H_2$ adsorbed at 15 K on H-SSZ-13 (previously outgassed at 773 K). The spectral sequence was obtained at increasing $H_2$ equilibrium pressures. First set of data (bottom part of the figure) ranges from $1 \times 10^{-7}$ up to 0.0025 bar; second set of data (top part of the figure) ranges from 0.0030 up to 0.013 bar. (a) $\nu$(OH) stretching region. Dashed and solid arrows refer to the isosbestic point and to the shoulder of unperturbed LF Brønsted sites, respectively. (b) $H_2$ stretching region (spectra are background subtracted). Red curve: IR spectrum of H-SSZ-13 outgassed at 773 K. Blue curves: effect of $H_2$ adsorbed at 15 K and at an equilibrium pressure of 0.0025 and 0.0030 bar. Magenta curve: effect of $H_2$ adsorbed at 15 K and at an equilibrium pressure of 0.013 bar. Black curves: intermediate coverages.

not only a contribution given by zeolite framework but also a contribution associated with specific interaction sites that in our case are the protons. This observation is of some interest because it is a peculiar property of zeolitic matrixes. Except when reactive defects are deliberately generated, in all other investigated microporous systems, $H_2$ seems to be adsorbed molecularly through dispersive interactions, and there is no evidence of any significant specific interaction between hydrogen and surface sites. Conversely, in the case of zeolites, there is evidence of specific interaction between $H_2$ molecules and cations. An evaluation of the number, distribution, and strength of specific interaction sites for $H_2$ can be obtained by IR spectroscopy in combination with low-temperature adsorption of small probe molecules.[35,36] Pioneering works of Kazansky and co-workers have shown that dihydrogen can be efficiently employed in low-temperature IR surface studies to reveal the presence of local electrostatic fields.[24,25] The perturbation of the $H_2$ molecule disrupts the local symmetry, making its stretching mode IR active (the more so the stronger the interaction). The resulting red shift of the frequency is also a measure of the strength of the interaction. When the polarizing species is a hydroxyl group, additional information on the interaction is disclosed by the $\nu$(OH) bands which are also strongly affected by the interaction.[26,35]

Figure 2 displays IR spectra of increasing doses of $H_2$ adsorbed on H-SSZ-13 at 15 K. Prior to the experiment, the sample was activated in vacuum at 773 K (see Materials and Experimental Section). Parts a and b cover the $\nu$(OH) and $\nu$(HH) regions, respectively. Before the diverse interactions between the zeolite and $H_2$ are discussed, some remarks should be made on the vibrational properties of H-SSZ-13. The spectrum of H-SSZ-13, represented by the red curve, shows a multiplicity of bands arising from different OH groups. The first family of bands (3750−3700 $cm^{-1}$) is assigned to $\nu$(OH) modes of weakly acidic silanol groups.[37] The second family of bands (3620−3570 $cm^{-1}$) represents strongly acidic Brønsted sites. The composite nature of this absorption has previously been ascribed to two superimposed contributions: a high frequency (HF) band at 3616 $cm^{-1}$ and a low frequency (LF) band at 3584 $cm^{-1}$. Due to the superposition on the tail of the HF component, the latter contribution gives the observed maximum at 3603 $cm^{-1}$.[38]

To clearly set out the spectroscopic changes that result from adsorbing hydrogen on the sample, the entire set of spectra has been divided into two series corresponding to two $H_2$ equilibrium pressure ranges. The lower series of spectra, obtained at low $H_2$ coverages (0−0.0025 bar), primarily describes interactions between $H_2$ and Brønsted sites belonging to the HF family, whereas the upper spectra, obtained at higher $H_2$ pressures (0.0030−0.013 bar), show the appearance of new types of interactions. The first series of spectra clearly demonstrates that hydrogen adsorption gradually decreases the intensity of the HF component. In parallel to this, a broad band representing $\nu$(OH) modes of Brønsted sites perturbed in OH···$H_2$ adducts grows around 3548 $cm^{-1}$ ($\Delta\nu_{O-H} = -64$ $cm^{-1}$). The presence of an isosbestic point (see dashed arrow in Figure 2a) is worth mentioning as it suggests formation of 1:1 adducts. In the last spectrum of the first series (blue curve), the LF band is still present (see solid arrow) as a shoulder on the left side of the perturbed OH band.

In addition to consuming the HF band, formation of OH···$H_2$ adducts leads to an activation of the $\nu$(HH) vibration of $H_2$, giving the bands in the region of 4160−4060 $cm^{-1}$ (unperturbed $\nu$(HH) mode appearing at 4161 $cm^{-1}$ in Raman spectra). Starting from low coverages, two bands with maxima at 4109 and 4090 $cm^{-1}$ can be seen (Figure 2b). The first component, growing in intensity in a parallel manner as the 3548 $cm^{-1}$ band, is inherently linked to the adduct formation between $H_2$ and the HF sites. The second component is less intense, even though it has a higher extinction coefficient, and must originate from a significantly less abundant family of sites.

In the second set of spectra, the $H_2$ pressure reaches a value sufficiently high to observe an erosion of the LF component at 3584 $cm^{-1}$. During the erosion of these Brønsted sites, the maximum at 3547 shifts to 3536 $cm^{-1}$. The shift toward lower frequency of the $\nu$(OH) component is the result of two phenomena. On one side, there is the contribution of LF species interacting very strongly with $H_2$, and on the other side, there is the condensation of $H_2$ inside the pores which causes a progressive shift to lower frequencies of the overall spectrum. This phenomenon is clearly evident in the last spectrum (magenta curve) obtained at 15 K with a $H_2$ equilibrium pressure of 0.013 bar. In the meantime, in the H−H stretching region (Figure 2b), mainly two phenomena can be observed: the growth of the sharp component at lower frequency, now at 4088

(35) Zecchina, A.; Spoto, G.; Bordiga, S. Vibrational Spectroscopy of Zeolites. In *Handbook of Vibrational Spectroscopy*; Chalmers, J. M., Griffiths, P. R., Eds.; John Wiley & Sons Ltd.: Chichester, U.K., 2002; Vol. 4, pp 3042−3071.
(36) Zecchina, A.; Otero Areán, C. *Chem. Soc. Rev.* **1996**, *25*, 187−197.
(37) Bordiga, S.; Ugliengo, P.; Damin, A.; Lamberti, C.; Spoto, G.; Zecchina, A.; Spanò, G.; Buzzoni, R.; Dalloro, L.; Rivetti, F. *Top. Catal.* **2001**, *15*, 43−52.
(38) Bordiga, S.; Regli, L.; Cocina, D.; Lamberti, C.; Bjørgen, M.; Lillerud, K.-P. *J. Phys. Chem. B* **2005**, *109*, 2779−2784.

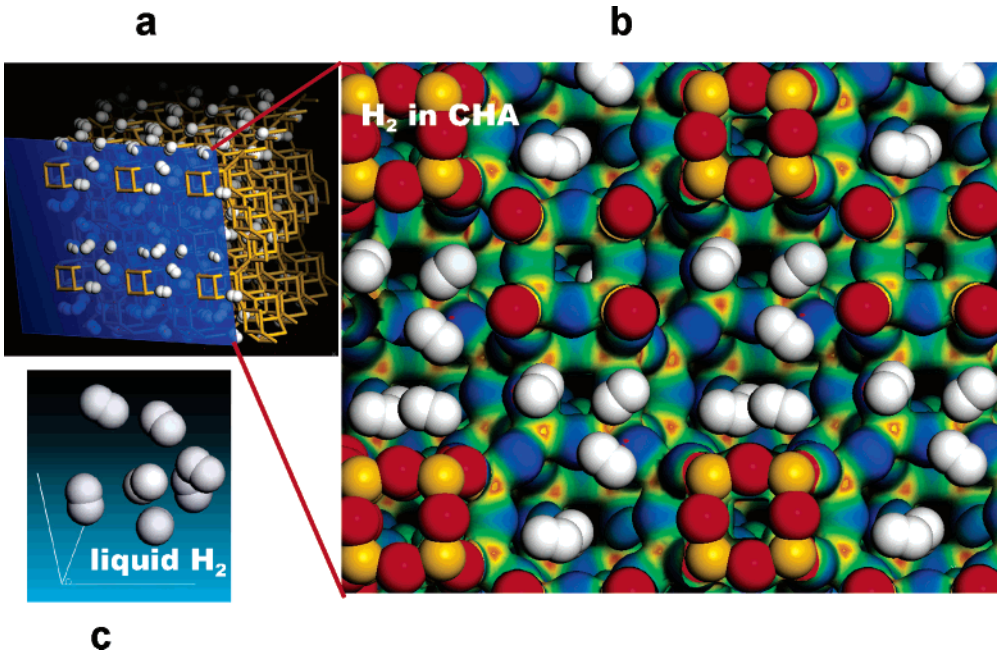


***Figure 3.*** Graphical representation of $H_2$ condensed in H-SSZ-13. (a) $H_2$ in H-SSZ-13 with the dihydrogen density resulting from the volumetric measurements performed on the material at 77 K and 0.92 bar (about five $H_2$ molecule per cage). The distribution of the adsorbate is the result of a molecular dynamics run performed at 298 K for 5 ps by means of the PCFF force field. The zeolitic framework is schematized representing only the links between the tetrahedral units. (b) Crystal slab defined by the blue plane of part a, with all of the atoms below the plane colored according to the electrostatic potential at the van der Waals surface (color scale: blue = negative values; red = positive values). Atoms above the plane are represented with CPK spheres (red: oxygens; yellow: silicons). (c) A model of liquid hydrogen at normal boiling point (20.39 K). In a volume equivalent to one CHA cavity, seven $H_2$ molecules are present, whose positions are obtained from a molecular dynamics run.

***Table 2.*** IR Frequency of $H_2$ Adsorbed in Different Protonic Zeolites or Zeotypes

| zeolite/zeotype | framework type (IZA code) | $\nu$(HH) ($cm^{-1}$) | $\nu$(OH)···$H_2$ ($cm^{-1}$) | ref |
|---|---|---|---|---|
| silicalite | MFI | 4130 | 3725 | unpublished results |
| H-Y | FAU | 4109 | 3601 | 25 |
| H-beta | BEA | 4107 | 3560 | unpublished results |
| H-ZSM-5 | MFI | 4103 | 3572 | 26 |
| H-FER | FER | 4103 | 3570 | unpublished results |
| H-MOR | MOR | 4102 | 3555 | 26 |
| H-SAPO-34 | CHA | 4096 | 3560 | unpublished results |
| H-SSZ-13 | CHA | 4090 | 3543 | this work |

$cm^{-1}$, and the appearance of a band at 4130 $cm^{-1}$ associated with slightly perturbed $H_2$. At this stage, a family of very strong acidic sites, most likely coupled to the LF band, appears to be involved in the interaction with $H_2$. The fact that these sites interact only at higher $H_2$ pressures may be explained by hypothesizing that they represent the sites that are not directly exposed at the 8-ring windows of the cages. In compliance with this, a separate analysis using CO as a probe molecule suggested that the HF component arises from OH groups located on the 8-rings, that is, the sites easily accessible for guest molecules.[38] The LF component was assigned to OH groups on the 6-rings forming the internal top or bottom of the barrel-shaped cage. The availability of these last sites is restricted, as they are partially coordinated to a framework oxygen. Finally, as already mentioned, at high loadings, hydrogen is condensed inside the nanovoids, forming a new phase. Under these circumstances, silanol groups are also interacting with hydrogen, as evidenced by the erosion of the band with a maximum at 3740 $cm^{-1}$ and the parallel growth of a broader absorption at 3718 $cm^{-1}$. A parallel experiment with H-SAPO-34 (not reported for brevity) has shown very similar results confirming the present assignment. To underline the rather extraordinary features of the OH···$H_2$ interactions in H-SSZ-13, a collection of data obtained for some protonic zeolites is reported in Table 2. Notice that only the CHA frameworks (H-SSZ-13 and H-SAPO-34) give a $\nu$(HH) frequency lower than 4100 $cm^{-1}$. All of the other zeolites, including highly acidic materials, such as H-beta and H-ZSM-5, interact more weakly with hydrogen and give higher $\nu$(HH) values, corresponding to smaller red shifts. This feature substantiates the peculiar affinity of the CHA framework toward $H_2$.

With the purpose of quantifying the adsorption energy of $H_2$ on the Brønsted acidic sites, isobaric IR experiments were performed at various temperatures. A known pressure of $H_2$ (57 mbar) was introduced to the cell, and spectra were then recorded at decreasing temperatures in the range of 300−15 K under equilibrium conditions. According to a method introduced by Paukshtis et al.,[39] the interaction energy can be derived from the temperature dependence of the intensity of the bands of the surface adducts. More recently, the method has been successfully adopted to describe the interaction of CO on MgO[33] and of $H_2$ in a Li-ZSM-5 by Otero Areán et al.[28] and of $H_2$ in a Na-ZSM-5 by Spoto et al.[29] In the present case, an adsorption energy of 9.7 ± 0.3 kJ $mol^{-1}$ was calculated. A specific $H_2$/surface interaction of about 10 kJ $mol^{-1}$ is rather remarkable, and similar values have been found only for $Na^+$-exchanged ZSM-5[29] (11 kJ $mol^{-1}$), whereas for Li-ZSM-5, an interaction energy of only 6.5 kJ $mol^{-1}$ has been obtained.[28] The adsorption energy of molecular hydrogen on graphite has been calculated to be about 4 kJ $mol^{-1}$, while for nanotubes, values about 9 kJ $mol^{-1}$ have been reported.[7] However, experimental measurements on nanotubes, fibers, and coals have shown adsorption energies lower

(39) Paukshtis, E. A.; Yurchenko, E. N. *Russ. Chem. Rev.* **1983**, *52*, 242−258.

than 5 kJ $mol^{-1}$.[40] Accurate calculations of the interaction energy with aromatic systems as models of graphitic nanoparticles and MOFs are also in this order of magnitude.[41] These values show that the acidic protons are good candidates as polarizing centers in the design of materials for hydrogen adsorption.

Finally, by considering liquid hydrogen, the available volume of a H-SSZ-13 cage may store seven hydrogen molecules (see Figure 3c). Our measured values indicate that at liquid nitrogen temperature, 57 K above the boiling point of hydrogen, about five hydrogen molecules are confined in each cage (see Figure 3a,b). This implies that we are close to hydrogen liquefaction inside the zeolitic nanovoids, a result which has never been obtained until now.

## 4. Conclusions

This contribution illustrates how broad experience in a specific class of materials combined with the use of well-known experimental techniques developed ad hoc leads to general inferences about how to promote hydrogen storage. The achieved results are interesting, not only because of the absolute values of $H_2$ uptake reached (which are remarkable without representing a new record for microporous materials) but also because they suggest structural and compositional features required for efficient hydrogen storage.

We have shown that proton-exchanged CHA frameworks represent promising materials where an appreciable interaction energy between hydrogen and specific surface sites, associated with a structure favoring physisorption, results in a relevant storage capacity. A proper balance between available space (volume accessible to hydrogen), high contact surface, and strong interaction with polarizing centers is the necessary characteristic requested to design better materials for molecular $H_2$ storage.

**Acknowledgment.** S. I. Zones is acknowledged for the private communication concerning the SSZ-13 synthesis. We are grateful to Laura Regli and Donato Cocina for help in the experiments. Regione Piemonte is acknowledged for financial support. M.B. is grateful for financial support from the Norwegian Research Council through Grant Number 158552/441.

JA050276C

(40) Schimmel, H. G.; Kearley, G. J.; Nijkamp, M. G.; Visserl, C. T.; de Jong, K. P.; Mulder, F. M. *Chem.—Eur. J.* **2003**, *9*, 4764−4770.
(41) Hübner, O.; Glöss, A.; Fichtner, M.; Klopper, W. *J. Phys. Chem. A* **2004**, *108*, 3019−3023.